Activationless Electron Transfer of Redox-DNA in Electrochemical Nanogaps

Zhiyong Zheng, Simon Grall, Soo Hyeon Kim, Arnaud Chovin, Nicolas Clement, Christophe Demaille

Activationless Electron Transfer of redox-DNA in Electrochemical Nanogaps

Zhiyong Zheng[1], Simon Grall[2], Soo Hyeon Kim[2], Arnaud Chovin[1], Nicolas Clement[2,3]*, Christophe Demaille[1]*

1 Université Paris Cité, CNRS, Laboratoire d'Electrochimie Moléculaire, F-75013 Paris, France

2 IIS, LIMMS/CNRS-IIS UMI2820, The University of Tokyo; 4-6-1 Komaba, Meguro-ku Tokyo, 153-8505, Japan

3 LAAS, 7 avenue du Colonel Roche, 31400 Toulouse, France

KEYWORDS: Nanoelectrochemistry, DNA nanoconfinement, reorganization energy, AFM-SECM, Q-Biol

ABSTRACT: Our recent discovery of decreased reorganization energy in electrode-tethered redox DNA systems prompts inquiries into the origin of this phenomenon and suggests its potential use to lower the activation energy of electrochemical reactions. Here, we show that the confinement of the DNA chain in a nanogap amplifies this effect to an extent where it nearly abolishes the intrinsic activation energy of electron transfer. Employing Electrochemical-Atomic Force Microscopy (AFM-SECM), we create sub-10 nm nanogaps between a planar electrode surface bearing end-anchored ferrocenylated DNA chains and an incoming microelectrode-tip. The redox cycling of the DNA's ferrocenyl (Fc) moiety between the surface and the tip generates a measurable current at the scale of ~ 10 molecules. Our experimental findings are rigorously interpreted through theoretical modeling and original molecular dynamics simulations (Q-Biol code). Several intriguing findings emerge from our investigation: (i) The electron transport resulting from DNA dynamics is many times faster than predicted by simple diffusion considerations. (ii) The current in the nanogap is solely governed by electron transfer rate at the electrodes. (iii) This rate rapidly saturates as overpotentials applied to the nanogap electrodes increase, implying near-complete suppression of the reorganization energy for the oxidation/reduction of the Fc heads within confined DNA. Furthermore, evidence is presented that this may constitute a general, previously unforeseen, behavior of redox polymer chains in electrochemical nanogaps.

INTRODUCTION

There is a growing consensus that confinement has the potential to modify the structure and functional properties of biomolecules.[1] Among the various length scales of confinement, nanoconfinement is attracting particular attention due to its similarity in dimension to molecules.[2] However, the exploration of nanospaces has been hampered by experimental challenges, such as the need for a practical method to construct nanogaps with high precision and controllability. Studying how nanoconfinement affects the behavior of DNA strands is of particular interest because it mimics the natural confinement of DNA within the molecular machinery of replication.[3] We aim to show that (nano)electrochemical studies of redox end-labeled DNA can notably provide relevant information in this field. When terminally attached to electrode surfaces, redox DNA oligonucleotides have also the interest of forming the sensing element of conformational electrochemical DNA (E-DNA) sensors.[4–8]. The electrochemical response of the redox-DNA strands is highly sensitive to bio-recognition events, which endows E-DNA sensors with superior sensitivity and selectivity for the detection of numerous analytes.[4,9–13] However, the molecular mechanisms behind this sensitivity are still under debate.[14] Proposed explanations include the modulation of either the dynamics of the DNA strand or the rate of electron exchange between the redox head of the strand and the electrode.[15–24] In a recent study focusing on ferrocene (Fc)-terminated short DNA strands,[25] we highlighted an additional and hitherto unsuspected contributing factor: the reorganization energy associated with the electron exchange. This parameter, which is related to the reorganization of water molecules around Fc after electron transfer, was found to be surprisingly low for ferrocene attached to the DNA strand end and also modulated (further diminished) by molecular recognition reactions. We hypothesized that this phenomenon was related to the remarkably high collision frequency of the DNA-bound Fc with the electrode, predicted by molecular dynamics simulations.[23,25] To test this hypothesis, we are now using an experimental setup that allows the nanoscale manipulation of the diffusion field of DNA-bound Fc molecules and the immediate determination of the Fc reorganization energy. Specifically, we confine the Fc-DNA strand within an electrochemical nanogap. This configuration holds immediate analytical interest because it provides an amplification mechanism that is lacking in "conventional" electrochemical DNA sensors. Namely, the chain's redox probe can be oxidized at one electrode and reduced at the other, i.e. undergo redox cycling, [26–29] so that a single redox probe exchanges many electrons consecutively. This principle has been successfully applied to the enhanced detection of "free" (unattached) redox molecules confined within electrochemical nanogaps a few tens of nanometers wide (sometimes less).[27,28,30–34] In the present case of immobilized redox DNA chains, the width of the nanogap has to be smaller than the ~ 10 nm length of the trapped DNA molecules to enable redox cycling. In this scenario, molecules are still free to move in a thin layer of electrolyte, but over length scales approaching their own dimension. This contrasts with related systems examined in molecular electronics, where the molecules are immobile and studied in the dry state.[35] Experimentally, such an "electrochemical molecular thin-layer cell" configuration has seldom been achieved, due to the difficulty in matching nanogap widths to molecular dimensions. In a rare exception, Lemay et al. have grafted linear ferrocenylated polyethylenglycol (PEG) chains to microfabricated electrodes forming planar nanogaps (65 nm in width).[36] Electron transport across the nanogap was demonstrated, but it involved electron exchange between the redox heads of the chains borne by each of the electrodes, because the PEG chains were too short to bridge the entire nanogap width.

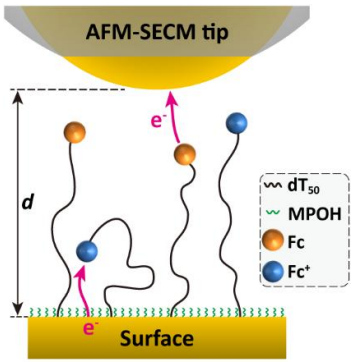

Figure 1. Schematic diagram of the redox cycling motion of the Fc heads in the nanogap between the AFM-SECM tip and the TS-Au surface. The Fc heads are tethered to the TS-Au surface through flexible DNA oligonucleotides, dT_{50}. The AFM-SECM tip potential, E_{tip}, is + 0.15 V vs. $E°$, while the surface potential, E_{sub}, is scanned cathodically. MPOH: 3-mercapto-1-propanol. The nanogap width, d, is defined as shown.

An even earlier exception has been our own work, where we used electrochemical atomic force microscopy (AFM-SECM) to confine redox-labeled, nanometer-long DNA chains in the nanogap formed by an ultramicroelectrode-tip and the DNA anchoring substrate electrode.[37,38] This work demonstrated the ability of end-attached redox-DNA chains to shuttle electrons across nanogaps, less than ~10 nm in width. However, quantitative information about the electron transport process could not be obtained due to the lack of a suitable model describing the motion dynamics of the confined DNA chains coupled to electron transfer events.

Such knowledge is now readily available through the molecular dynamics software Q-Biol, which we have been developing.[39] Hence, the present work aims to systematically investigate, aided by Q-Biol, the electrochemical behavior of a diluted layer of Fc-terminated dT oligonucleotides (dT_{50}) end-anchored to a gold electrode, confined and probed by an AFM-SECM tip. The main goal is to achieve a complete fundamental understanding of electron transport by the Fc-DNA chains across nanogaps, with a particular focus on accessing the reorganization energy associated with the redox cycling of the Fc head. Unexpected properties are revealed: (i) Electron transport by DNA dynamics across nanogaps is several orders of magnitude faster than predicted from mere diffusional considerations, (ii) the nanogap current is controlled solely by the electron transfer rate at electrodes, (iii) this rate saturates at relatively low overpotentials applied to the confining electrodes (i.e., tip and substrate), indicating an almost complete suppression of the reorganization energy for the oxidation/reduction of the Fc heads of confined DNA. Evidence is presented that this may constitute a general, so far unsuspected, behavior of redox polymer chains confined to electrochemical nanogaps.

RESULTS

Redox-DNA layer assembly and AFM-SECM approach curve

Fc-dT_{50} was 5' thiol-anchored to the surface of an ultra-flat template-stripped gold surface (TS-Au) in the presence of 3-mercapto-1-propanol (MPOH), used as a surface diluent preventing flat-lying adsorption of the oligonucleotides.[40] Note

that MPOH was preferred to the longer and more conventionally used mercaptohexanol (MCH) diluent, as MPOH enables a faster rate of electron transfer to the electrode for Fc-DNAs.[25] As detailed previously, this led to a low-density Fc-dT$_{50}$ layer, characterized by an almost ideal surface cyclic voltammetry (CV) signal, at slow scan rates, $v \leq 1$ V/s, Figure S1. Integration of the CV yielded a surface coverage of $\Gamma = 2 - 3$ pmol/cm^2 and a standard potential, $E°$, of + 0.17 ± 0.01 V/SCE, in agreement with previous work.[25,41] The chain coverage translated into an average interchain separation ($1/\sqrt{\Gamma}$) of ~7 -9 nm. Being comparable to the Flory radius of dT$_{50}$ in solution (8-10 nm),[42–44] the separation was large enough for the Fc-dT$_{50}$ chains to behave independently, i.e. with minimal chain-chain interactions.

End-anchored Fc-dT$_{50}$ chains were locally confined to nanogaps of controllable widths, d, by approaching the AFM-SECM probe to the gold surface (substrate), in-situ (in a pH 7, phosphate buffered $NaClO_4$ 1M electrolyte), Figure 1. The potentials of the tip and substrate, E_{tip} and E_{sub} were controlled and initially set to be positive (anodic) and negative (cathodic) versus $E°$, respectively. During the approach, both force and electrochemical current raw-approach curves were simultaneously recorded (Figure S3).[37,45] This allowed the dependence of the tip current, i_{tip}, on the tip-substrate distance, d, to be accurately obtained, Figure 2.

The onset of the electrochemical current was detected when

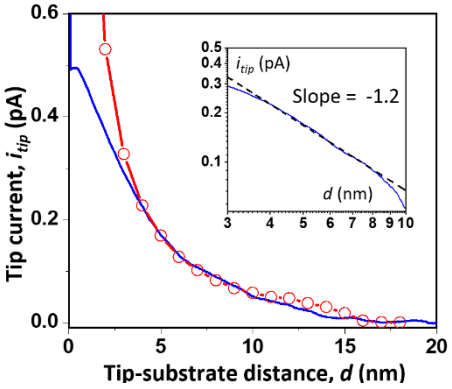

Figure 2. AFM-SECM approach curve recorded on an end-anchored Fc-dT$_{50}$ layer. Fc-DNA is confined within the tip-substrate nanogap of width d. The experimental curve is shown in blue and the theoretical curve, calculated with eq 1, in red. The inset is a Log vs. Log plot of the approach curve evidencing its approximate $1/d^{1.2}$ behav-

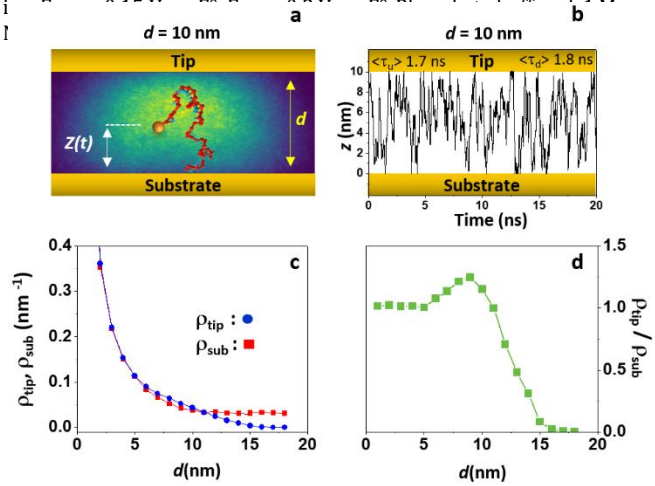

Figure 3. Q-Biol molecular dynamics simulations. (a) Snap shot of the Fc-dT$_{50}$ chain confined in an electrochemical nanogap of width d = 10 nm. (b) ~20 ns of a ~10 µs time-trace tracking the position of the Fc head in the gap. The average times for the Fc head to go from the substrate to the tip (τ_u) or conversely (τ_d) are shown. (c) Probability of presence of the Fc head at the tip, ρ_{tip}, or at the substrate, ρ_{sub}, as a function of the nanogap width. (d) ρ_{tip} / ρ_{sub} ratio vs. gapwidth.

the tip was ~15 nm away from the surface, a distance falling between the statistical end-to-end radius of dT$_{50}$ (~ 7 nm) and the full chain contour length (35 nm).[46] The current then increased as the tip was brought closer to the surface, until a sharp rise due to tunneling was recorded, typically for d < 1nm. In the d = 1-15 nm region, the current was generated by the redox cycling of the Fc-heads of the chains, which, as a result of chain motion, came alternatively in contact with the tip and substrate, where they were respectively oxidized and reduced, Figure 1. Interestingly, we noticed that it was sufficient to bias the tip and surface at potentials only modestly remote from $E°$ for the tip current to become independent of their exact values. This required $E_{tip} \geq$ + 0.15 V vs. $E°$, $E_{sub} \leq$ - 0.2 V vs. $E°$. The aforementioned data corresponds to this situation.

In order to assess the contributions of the DNA chain motion and of the electron transfer rate at the electrodes to the kinetic control of the tip current, we made use of the Q-Biol code, developed in our previous works.[25,39] Q-Biol is based on OxDNA[47], a nucleotide-level coarse-grained molecular dynamics model of DNA. It accurately reproduces the DNA chain motion and electron transfer events at the confining electrodes, Figure 3a.[39]

Time traces were constructed by tracking the vertical position (Z) of the Fc head in the nanogap, Figure 3b. They showed that the collision frequencies of the Fc head with the tip and the substrate were in the order of nanoseconds. This is three orders of magnitude faster than one could predict based on the diffusion properties of the unconfined (and unattached) DNA chain.[48–50] Such fast collision dynamics originate from the confinement of the Fc-head "diffusion" path to a nanometer-sized hemispherical domain, defined by the length of tethering chain.[25] Similarly high collision frequencies were also derived from random walk simulations for the diffusion of a species confined to an electrode surface by a hemispherical cap.[23] In the particular case explored here, this phenomenon provides an unprecedentedly fast transport mechanism for shuttling redox electrons across the nanogap. As a result, chain motion cannot be the only factor kinetically controlling the current generation. Indeed, such fast DNA dynamics would theoretically generate currents in the hundreds of pA, whereas sub-pA-range currents were typically recorded in AFM-SECM for end-attached Fc-dT layers, Figure 2.[39,51] Besides, in the diffusive scenario, approach curves are predicted to display a pronounced $1/d^2$ signature (Figure S8), whereas the actual curves vary coarsely as $1/d$ (inset in Figure 2).

Potential dependence of the tip-current

Further studying the electron transfer properties of nanogap-confined redox DNA requires that the complete potential dependence of the current is investigated. Thus, we carried-out a sequence of controlled step-by-step approaches of the tip toward the surface, stopping at fixed nanogap widths, where the substrate potential was scanned from -0.2 V vs. $E°$ toward +0.17 V vs. $E°$ and back, at 20 mV/s, Figure S5. The tip was biased at a potential anodic enough for the current to be independent of its value (+0.15 V vs. $E°$). The advantage of scanning the substrate potential instead of the tip potential was that no interfering capacitive tip current was generated. This enabled well-defined tip current, i_{tip} vs. E_{sub} CVs to be recorded for various nanogap widths, Figure 4a. Note that the nanogap width was calibrated from current approach curves recorded in sequence with the CVs, affording a reliable determination of d to within ± 1nm, see Section 1C in Supporting Information. The substrate current was also simultaneously

recorded as a control, providing an i_{sub} vs. E_{sub} CV usable as an un-ambiguous "in situ" potential reference, Figure 4b. Note that for these CVs, all the chains present on the surface are addressed, so the contribution of the redox cycling of the few chains located below the tip is negligible.

In Figure 4a, one can first observe that the i_{tip} vs. E_{sub} CVs were S-shaped, displaying a well-defined current plateau. This evidenced the purely faradaic nature of the current, with no interference from long-range tunneling current, which would make the current grow exponentially with the biais.[52] Moreover, the forward and backward traces of the CVs were almost superimposable, which showed that the nanogap width did not vary during their recording.[53] Forward traces were therefore studied in the following analysis. The intensity of the plateau current increased when d decreased, following the current approach curve shown in Figure 2.

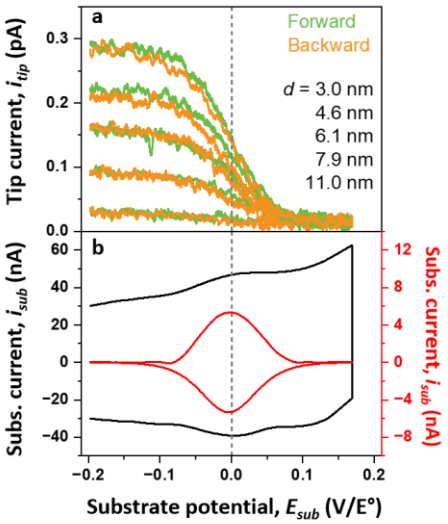

Figure 4. Electrochemical responses of end-attached and nanoconfined Fc-dT$_{50}$ upon scanning the surface potential, *Esub*. (a) Tip CVs, i_{tip} vs. E_{sub}, recorded at different nanogap widths, d. (b) Simultaneously recorded i_{sub} vs. E_{sub} surface CVs. Raw and background-subtracted CVs are shown in black and red traces, respectively. E_{sub} was scanned at 20 mV/s from -0.20 to +0.17 V vs. $E°$ and back. E_{tip} = + 0.15 V vs. $E°$. Phosphate buffered, 1 M $NaClO_4$ aqueous electrolyte, pH = 7. T = 25°C. Coverage Γ = 2.5 pmol/cm^2.

A remarkable feature of these CVs was that their shape, and even more importantly their position along the potential axis, did not depend on d. This peculiar trend was quantified by plotting the value of the half-wave potentials, $E_{1/2}$, of a large series of CVs (forward curves, Figure 5a), recorded at various nanogap widths, as a function of d, Figure 5b. One could observe that $E_{1/2}$ values were almost d-independent, at least for d < 9 nm. Also remarkable was the fact that, within experimental errors, $E_{1/2}$ values were close to $E°$ in this nanogap width region. Importantly, identical results were obtained when decreasing the ionic strength of the electrolyte by a factor of two (down to 0.5 M), ruling out the contribution of electrostatics to the CV response, Figure S6. This result may seem surprising, considering the substantial charge (~30 e$^-$)[54] of the dT$_{50}$ chain, and also knowing that the effects of the electrochemical double layer on redox cycling in nanogaps of multiply charged redox molecules have been reported.[34,55–57] However, the situation here is different because it's not the redox label that carries the charge, but the DNA chain. Besides, we observed that neutral, end-grafted Fc-PEG$_{3400}$ chains behaved in a way similar to Fc-DNA chains when confined in AFM-SECM nanogaps: they also displayed i_{tip} vs. E_{sub} CVs characterized by very small, distance-independent $E_{1/2}$ - E_0 values (Figure S7).[58] This points to a general and unsuspected property of confined polymeric redox systems.

Overall, the above-described CV behavior observed for confined Fc-DNA (and Fc-PEG) chains are in striking contrast with that reported for freely diffusive species trapped in nanogaps, where the CV shifted toward higher overpotential regions as the nanogap was closed.[59] This shift was indicative of mixed kinetic control of the current by the rate of diffusion and that of electron transfer, a scenario we can thus definitely exclude in the context of the present study.

One is thus led to conclude that the current is here under the *sole* control of the electron transfer steps, a situation never previously documented in nano-electrochemistry.

Quantitative analysis of the approach curves and CVs : derivation of the electron transfer kinetic parameters

From the above analysis, it can be inferred that the intensity of the tip current depends on the rate constants of the electron transfers at both the tip and the substrate, weighted by the presence probability of the Fc head at their surfaces. The S-shaped CVs presented in Figures 4 and 5 translate the potential dependence of the rate of electron transfer at the substrate.

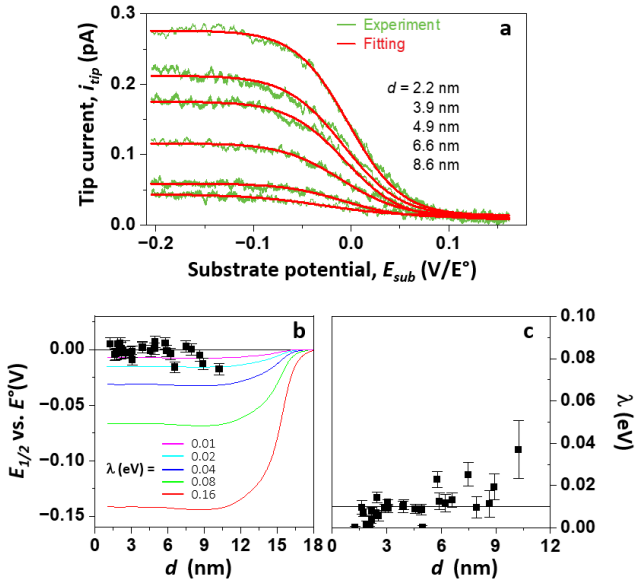

Figure 5. Electrochemical characteristics of Fc-dT$_{50}$ confined under nanogaps of various widths, d. (a) Raw tip CV (forward traces, greentraces) recorded at various d and corresponding best-fit curves from the MHLC model, calculated with $E_{1/2}$ = 0 V vs. $E°$ and λ as the sole adjustable parameter (red traces). (b) Experimental $E_{1/2}$ and (c) best fit reorganization energy values, λ, as a function of d. Error bars in (b) and (c) correspond to the experimental error on $E_{1/2}$ determination and the standard error on the best-fit λ values, respectively. E_{tip} = + 0.15 V vs. $E°$. Phosphate buffered, 1 M $NaClO_4$ aqueous electrolyte, pH = 7. T = 25°C. E_{sub} scan rate 20 mV/s.

The plateau current of the CVs corresponds to the saturation of the rate of electron transfer at high enough substrate and tip overpotentials, a feature uniquely predicted by the Marcus-Hush-Levich-Chidsey (MHLC) model of electron transfer kinetics.[60–62] The plateau current is thus given by:[39].

$$i_{tip}^{pl} = Ne\frac{k_{tip}^{\infty}\rho_{tip}k_{sub}^{\infty}\rho_{sub}}{k_{sub}^{\infty}\rho_{sub}+k_{tip}^{\infty}\rho_{tip}} \quad (1)$$

N is the number of Fc-DNA chains involved and *e* the elementary charge. k_{tip}^{∞} and k_{sub}^{∞} are the heterogeneous electron transfer rate constants at infinitely large overpotentials at the tip and substrate, respectively. ρ_{tip} and $\rho_{sub}$are the probability of presence of the Fc head at the tip and substrate, respectively.

This equation can be obtained from "classical" expressions for the electrochemical current in a nanogap, when mass transport is much faster than the rate of electron transfer at the electrodes (see Section 2E in Supporting Information). [59]

Due to its fast dynamics, the chain conformation is always at equilibrium and ρ_{tip} and ρ_{sub} can be derived from the time-averaged simulations for any nanogap width, *d*. The dependence of ρ_{tip} and ρ_{sub} on *d* are presented in Figure 3c. As expected, for d > 15 nm, ρ_{tip} tends toward zero as the chain cannot touch the tip, while ρ_{sub} is relatively low due to the surface-avoiding behavior of the chain. Upon closing the nanogap, both presence probabilities increase and become comparable for $d \leq 5$ nm.

From the simulated ρ_{tip} and ρ_{sub} dependence on *d*, a theoretical current approach curve (i.e. plateau current vs. *d*) could be calculated using equation (1). For this we considered $k_{sub}^{\infty} = k_{tip}^{\infty}/3$, since we evidenced that the rate of electron transfer of the soluble species ferrocenedimethanol (analogous to the Fc heads) at a gold electrode was slowed by a factor of 3 by the presence of a MPOH layer, Figure S2. Using the term Nk_{tip}^{∞}as the sole adjustable parameter then enabled a good agreement between the theoretical and experimental current approach curves to be obtained, down to $d \sim 3$ nm, yielding a best-fit value of Nk_{tip}^{∞} = 4 cm/s (red trace in Figure 2). Deviation from the fit for d < 3 nm can be attributed to the complex behavior of over-confined DNA chains (onset of ballistic motion, thermal effects),[39] which was ignored here. Comparing the radius of the AFM-SECM tips (20-50 nm) to the interchain separation (~8 nm) one can conclude that about *N* ~ 10 chains may be contacted by the sharp tip, yielding $k_{tip}^{\infty} \sim$ 0.4 cm/s.

The whole i_{tip} vs. E_{sub} CVs can be accounted for by considering the potential-dependence of the electron transfer rate constant at the substrate, k_{sub}, expressed in the framework of the MHLC model:[60–62]

$$\frac{k_{sub}(\xi_{sub})}{k_{sub}^{\infty}} = \frac{1}{\sqrt{4\pi\lambda^*}}\int_{-\infty}^{\infty}\frac{exp\left[-\frac{\left(\lambda^*+\xi_{sub}-x\right)^2}{4\lambda^*}\right]}{1+exp\,(x)}dx \quad (2)$$

with $\xi_{sub} = F(E_{sub} - E°)/RT$ and $\lambda^* = F\lambda/RT$, Figure S9.

ξ_{sub} and λ^* are the normalized overpotential and reorganization energy associated with the reduction of the Fc^+ head, respectively.

Generalizing eq 1 for any ξ_{sub} value, and using eq 2 to express the electron transfer rates, yields the theoretical equation for the i_{tip} vs. E_{sub} CV, normalized by its plateau current, $i_{tip,pl}$ (see Section 2D in Supporting Information):

$$\frac{i_{tip}}{i_{tip,pl}} = \frac{1+\Lambda^*}{1+e^{\xi_{sub}}+\frac{\Lambda^*}{f(\xi_{sub},\lambda^*)}} \quad (3)$$

where $f(\xi_{sub},\lambda^*) = k_{sub}(\xi_{sub})/k_{sub}^{\infty}$ and $\Lambda^* = k_{tip}^{\infty}\rho_{tip}/k_{sub}^{\infty}\rho_{sub}$.

In the general case, the corresponding dimensionless CV depends on the values of both λ* and Λ*, and can be calculated numerically from eq 3, Figure S12. The dependence of its half-wave potential on λ* and Λ* is shown in Figure S13. For a given λ* value, the *d* – dependence of the CV is captured by a single parameter, Λ*. Upon approaching the tip to the surface, Λ* goes from zero (since ρ_{tip} = 0 at large *d*) toward a constant value of $\Lambda^* = k_{tip}^{\infty}/k_{sub}^{\infty}$ at small gaps, since $\rho_{tip} = \rho_{sub}$when *d* is small, Figure 3d. The simulated ρ_{tip} and ρ_{sub} dataset of Figure 3 enables Λ* to be derived at any *d,* and thus theoretical CVs to be calculated for any gap width. Figure 5b shows the variation of $E_{1/2}$ of such Cvs as a function of *d,* calculated from eq 3 for a series of λ values (colored traces).

It can be seen that, the $E_{1/2}$ value is predicted to be equal to $E°$ when the tip barely makes contact with the chain ($d \geq 15$ nm, Figure 5b). In this situation the electron transfer at the tip is very slow while it is at equilibrium at the substrate. Consequently, the current is then immeasurably small. However, as the tip is approached further to the substrate, $E_{1/2}$ is expected to rapidly shift negatively, reaching a *d*-independent value from *d* ~12 nm and below. One can see that this limiting $E_{1/2}$ value depends on λ, being more negative the higher λ is. Actually, $E_{1/2}$ - $E°$ then approaches a value of –λ (Figure S13). This illustrates how the reorganization energy associated with rate-limiting electron transfers in nanogaps can be immediately "visually" estimated from the $E_{1/2}$ of i_{tip} *vs.* E_{sub} *(or* E_{tip}*)* CVs.

Our experimental observation of a wide *d* region, ranging from ~2 – 11 nm, where $E_{1/2}$ values were found to be *d*-independent, fully complies with the above prediction.

This result confirms that the electron transfer steps at the electrodes alone control the current recorded at nanogaps confining end-attached, redox-labeled DNA chains.

Moreover, considering again Figure 5b, the large set of experimental $E_{1/2}$ values, once reported on the family of theoretical curves, lead to *an exceedingly small* λ value of 0.04 eV or less.

Similarly, fitting the individual i_{tip} vs. E_{sub} CVs with equation (3), using λ as the sole adjustable parameter, yielded λ values distributed around 0.01 ev for $d \leq 9$ nm, Figure 5c. A subtle trend of an increase of λ with *d* can be observed for $d > 9$. This could be due to a gradual transition from the confined regime to that of a DNA chain simply end-attached (unconfined), which is characterized by a higher λ value (see below).[25]

Finally, it should be noted that a low value of λ is required to justify our first qualitative observation that the tip current became independent of the overpotentials applied to the tip and the surface once these exceeded a few hundred millivolts only. Indeed, the MHLC model predicts that the electron transfer rate constant reaches a saturation value for lower overpotential values the smaller lambda is, see Figure S9.

DISCUSSION

Our measurement of an extremely small λ value for the Fc head of confined DNA, compared to the admitted value for the reorganization energy of Fc (0.85 eV) (Figure S2),[60] falls in line with our previous demonstration that the electrochemical response of (unconfined) Fc-$(dT)_N$ (N = 10-50) chains, end-grafted to gold surfaces, was characterized by very low reorganization energy values, (~ 0.2 eV for Fc-dT_{50}). This was the first evidence that the attachment of the Fc head to a DNA chain, terminally immobilized on an electrode surface, contributes to a large decrease in λ. The present study evidences that the reorganization energy is further reduced and almost completely suppressed when the terminally attached Fc-DNA chain is also confined. The fact that a decrease in λ was observed for two different chain configurations (unconfined or confined), using two different techniques (transient CV or stationary AFM-SECM) addressing a very different number of molecules (millions or ~ 10), strongly supports our assertion that the reorganization energy is greatly reduced in Fc-DNA systems. We can only assume that this effect is related to the polymeric nature of the DNA chain and its coiling behavior. The fact that it is more pronounced for confined vs. unconfined DNA would point to a role of the conformational energy of the chain, which is modulated by the confinement in the nanogap.

In our previous study of unconfined, surface-attached Fc-DNA,[25] we suggested that our results could be understood based on the expression of λ_o, the solvent reorganization energy, equation 4 : [61]

$$\lambda_0(z) = \frac{e^2}{8\pi\varepsilon_0}\left(\frac{1}{\varepsilon_{op}} - \frac{1}{\varepsilon_s}\right)\left(\frac{1}{a_0} - \frac{1}{2(z+a_0)}\right) \qquad (4)$$

where a_0 = 0.38 nm is the Fc radius, z the distance to the electrode, ε_{op} = 1.78 is the relative water permittivity at optical frequency, ε_s the relative water permittivity of water at the frequency of molecule motion (~80 in the bulk).

The total reorganization energy (λ) determined here is the sum of the solvent (λ_0) and internal (λ_i) reorganization energies, but for ferrocene λ_i was predicted to be very small ~0.016 eV. [63]

Our observation of a reduced λ value would thus mostly arise from a decrease of λ_0, ascribable to a lowering of the ε_s value, tending toward that of ε_{op}. At a microscopic level, several factors could be at the origin of a low ε_s value, including the entrance of Fc in the Stern layer due to the inertial motion of DNA,[39] the Stern layer having a very low dielectric constant.[64] This effect would be consistent with the recent observation that redox molecules rigidly immobilized on electrodes, close enough to the surface to be permanently inside the electric double layer, exhibit small λ_0 values.[65] Other factors could here be the high-frequency motion of Fc, which is in the range of water dielectric relaxation, or contributions from the DNA chain itself, which may participate in the solvation of Fc. In addition, the dielectric constant of water confined in nanometer-wide nanogaps is known to be lowered,[66] so this effect may also play a role here. In any case, the attachment of a redox moiety to a DNA chain and its confinement within a nanogap appears to be a completely unexpected way to modulate and even suppress the activation energy of electron transfer.

The value found above for k_{tip}^{∞}, is also worth discussing. A general and workable theoretical formulation for k^{∞} is :[62]

$$k^{\infty} = Z\kappa_e$$

Z is the collision factor, in cm/s, given by: $Z = \sqrt{RT/2\pi M}$, with M the molar mass of the redox species. κ_e is the transmission coefficient (ranging from 0-1). κ_e depends on the electronic coupling energy parameter, H and on λ as:[62]

$$\kappa_e = \frac{2 - 2\exp\left[-1.35\ 10^3\ H^2/\sqrt{\lambda}\right]}{2 - \exp\left[-1.35\ 10^3\ H^2/\sqrt{\lambda}\right]}$$

where H and λ are expressed in eV and a temperature of 25°C is assumed. κ_e is plotted vs. λ and H in Figure S11.

For a freely diffusing small redox molecule, such as ferrocenedimethanol, Z ~5 10^3 cm/s , λ = 0.85 eV and H >0.1 eV,[67] so that κ_e~1. k^{∞} is thus in this case in the order of 10^3 cm/s.

The corresponding value we obtained here for of Fc-DNA (k_{tip}^{∞} = 0.4 cm/s) is ~3 orders of magnitude smaller. This can be understood as a significantly smaller H-parameter value for the DNA-attached vs. free ferrocene. A likely scenario is that the attachment of the Fc head to the DNA chain limits the possible orientations of the Fc with respect to the surface, which would affect (statistically reduce) the electronic coupling energy. We have previously reported quantum chemistry simulations which evidenced such a large dependence of the electronic coupling energy on the angstrom-scale positioning of Fc.[68] Of note, the reduction in λ upon passing from free Fc to Fc-DNA would have been expected to actually increase the k_{tip}^{∞} value, but this effect is likely dwarfed by the much sharper dependence of κ_e on H than on λ, Figure S11.

CONCLUSION

AFM-SECM, combined with state-of-the-art molecular dynamics simulations, allowed us to decipher the electron transport by end-attached redox DNA chains across electrochemical nanogaps of molecular dimensions.

We reveal that, as a result of its hemispherical motional field, the collisional dynamics of the redox head with the confining nanogap electrodes is several orders of magnitude faster than expected from mere diffusion. Consequently, the nanogap current is under full kinetic control by the electron transfers at the electrodes, an unprecedented situation for an electrochemical nanogap. Most importantly, the potential dependence of the current most-visibly evidences a saturation of the electron transfer rates at unexpectedly low overpotential values. Based on the Marcus-Hush-Levich-Chidsey model of electron kinetics transfer kinetics, we show that this behavior is ascribable to an almost complete suppression of the activation energy of the electron transfer of the Fc head at the nanogap electrodes. Such a phenomenon is tentatively attributed to modulation of the solvent reorganization energy term of Marcus equations, resulting either from the extremely fast dynamics of the DNA-borne Fc, the inertial motion of the DNA chain, or its contribution to the solvation of the Fc. In any case, our results imply that future nanogap-based E-DNA sensors could operate under very low overpotentials. Our work provides a solid quantitative basis for the understanding of the transduction mechanism of these nanodevices. Furthermore, we also showed that the suppression of the activation energy in nanogaps is not limited to Fc-DNA chains, since we also observed it here for Fc-PEG chains. Thus, this may be a general, previously unforeseen property of redox polymer chains confined in electrochemical nanogaps that could be exploited for important applications in e.g. electrocatalysis.

MATERIALS AND METHODS

Materials. Doubly HPLC purified, custom functionalized oligonucleotides (oligo-dT), bearing a redox ferrocene (Fc) label at their 3' end and a disulfide group at their 5' extremity, were acquired from Eurogentec (Belgium). Their structure and conditioning were as described previously.[25] All other chemicals and solvents were analytical grade and used as received.

Assembly of the Fc-dT_{50} layer. The assembly of the Fc-dT_{50} layer has been described in detail elsewhere.[25] Briefly, the Fc-oligonucleotide-disulfide was reduced to its free thiol form just before grafting using tris(2-carboxyethyl)phosphine) (TCEP). MCH (6-Mercapto-1-hexanol), released as a by-product of the reduction reaction, was separated from the Fc-oligonucleotide-thiol by using an oligo clean-up and concentration kit (Norgen Biotech). 1-Propanethiol (termed MPOH), prepared in 360 mM PBS (88.6 mM NaH_2PO_4, 271.4 mM Na_2HPO_4, 990 mM NaCl, pH 7.4) was added to the purified oligonucleotide. The final concentrations of Fc- dT_{50} and MPOH in the adsorption solution were both of 20 µM. A Teflon mask was used to delimitate a 4 mm diameter disk-shaped region on a freshly exposed template-stripped ultra-flat gold surface (TS-Au).[69] A 20 µL drop of the Fc-DNA/MPOH solution was deposited on this area and the incubation lasted overnight. After thorough rising with the electrolyte (1 M $NaClO_4$, 10.6 mM NaH_2PO_4, 14.4 mM Na_2HPO_4, pH 7.0), the surface was mounted as the bottom electrode in an electrochemical fluidic cell, prior to carrying out the cyclic voltammetry (CV) and atomic force electrochemical microscopy (AFM-SECM) analyses.

Assembly of Fc-PEG_{3400} layer. Home-synthesized, linear Fc-PEG_{3400}-disulfide was used to form end-grafted Fc-PEG layers on TS-Au as described in our previous works. [70]

AFM-SECM and CVs characterizations. AFM-SECM characterizations were performed as described previously.[25,51] Combined atomic force-electrochemical tips home-made from gold wires, and displaying a radius of 20 – 50 nm and a spring constant in the order of 1N/m, were used. The experiments were carried out using a JPK Nanowizard II microscope, connected to a homemade bipotentiostat, operated in a four-electrode configuration. The tip and the surface carrying the Fc-DNA (substrate) were the two working electrodes. A platinum coil and a home-prepared polypyrrole-coated platinum wire (calibrated vs. KCl saturated calomel electrode, SCE) acted as the counter and reference electrodes, respectively. The bipotentiostat enabled the tip and substrate potential to be independently applied (E_{tip} and E_{sub}, respectively) and scanned, while the tip and substrate current (i_{tip} and i_{sub}, respectively) were recorded.

Integration of the slow scan rate i_{sub} vs. E_{sub} CVs (1 V/s or slower) yielded the molar amount of Fc-DNA chains present on the surface, N_0, and the standard potential of the Fc labels of the end-anchored DNA chains, $E°$. All of the potentials given in this work are expressed vs. $E°$, unless otherwise stated. Dividing N_0 by the *geometric* surface area of the electrodes, S, yielded the chain coverage, Γ.

ASSOCIATED CONTENT

Supporting Information

Extra CV and AFM-SECM results and protocols: i_{sub} vs. E_{sub} CV characterization of the Fc-DNA layer. Measurement of the standard heterogeneous electron transfer rate constant and reorganization energy for Ferrocenedimethanol at a MPOH-coated Au electrode. Deriving i_{tip} vs. d curves from simultaneous force and current approach curves. The sequence of tip motion and E_{sub} scanning operations to record i_{tip} vs. E_{sub} voltammograms at various d. Effect of lowering the $NaClO_4$ electrolyte concentration to 0.5 M on the i_{tip} vs. E_{sub} CV. i_{tip} vs. E_{sub} CVs acquired at an Au-TS surface bearing a Fc-PEG layer. Theory: Tip current approach curve expected in the case of kinetic control by chain dynamics. Dependence of the electron transfer rate constant and the k_s/k^∞ ratio as a function of the overpotential and reorganization energy. Dependence of k^∞ on the electronic coupling and reorganization energies. Derivation of the eq 1 and 3. Comments on the use of Equation S1 versus more classical electrochemical equations to derive nanogap currents. The Supporting Information is available free of charge on the ACS Publications website.

AUTHOR INFORMATION

Corresponding Authors

Dr. Christophe Demaille - Université Paris Cité, CNRS, Laboratoire d'Electrochimie Moléculaire, F-75013 Paris, France. E-mail: Christophe.demaille@u-paris.fr.

Dr. Nicolas Clément - IIS, LIMMS/CNRS-IIS UMI2820, The University of Tokyo; 4-6-1 Komaba, Meguro-ku Tokyo, 153-8505, Japan. E-mail: nclement@iis.u-tokyo.ac.jp.
LAAS, 7 avenue du Colonel Roche, 31400 Toulouse, France nclement@laas.fr

Author Contributions

C. Demaille and N. Clément obtained the funding, supervised the project and designed the experiments. Z. Zheng conducted the CV characterizations and analyzed the results. A. Chovin designed the AFM-SECM setup and initial experiments, and trained Z. Zheng to conduct them. C.S.H. Kim provided scientific interactions on DNA nanoelectrochemistry and related simulations. S. Grall conducted Q-Biol simulations. C. Demaille, N. Clément and Z. Zheng co-wrote the paper with scientific interpretation and comments from all authors.

Notes

The authors declare no competing financial interests.

ACKNOWLEDGMENT

This work has received financial support from the French "Agence Nationale de la Recherche" (ANR), through the "SIBI" project (ANR- 19-CE42-0011-01), and from the Unicorn-Dx EU-Attract project.

REFERENCES

(1) Liu, W.; Stoddart, J. F. Emergent Behavior in Nanoconfined Molecular Containers. *Chem* **2021**, *7* (4), 919–947. https://doi.org/10.1016/j.chempr.2021.02.016.

(2) Wordsworth, J.; Benedetti, T. M.; Somerville, S. V.; Schuhmann, W.; Tilley, R. D.; Gooding, J. J. The Influence of Nanoconfinement on Electrocatalysis. *Angew. Chemie - Int. Ed.* **2022**, *61* (28), e202200755. https://doi.org/10.1002/anie.202200755.

(3) Cramer, P.; Bushnell, D. A.; Fu, J.; Gnatt, A. L.; Maier-Davis, B.; Thompson, N. E.; Burgess, R. R.; Edwards, A. M.; David, P. R.;

Kornberg, R. D. Architecture of RNA Polymerase II and Implications for the Transcription Mechanism. *Science (80-.).* **2000**, *288* (5466), 640–649. https://doi.org/10.1126/science.288.5466.640.

(4) Lubin, A. A.; Plaxco, K. W. Folding-Based Electrochemical Biosensors: The Case for Responsive Nucleic Acid Architectures. *Acc. Chem. Res.* **2010**, *43* (4), 496–505. https://doi.org/10.1021/ar900165x.

(5) Du, Y.; Dong, S. Nucleic Acid Biosensors: Recent Advances and Perspectives. *Anal. Chem.* **2017**, *89* (1), 189–215. https://doi.org/10.1021/acs.analchem.6b04190.

(6) Ferapontova, E. E. DNA Electrochemistry and Electrochemical Sensors for Nucleic Acids. *Annu. Rev. Anal. Chem.* **2018**, *11* (1), 197–218. https://doi.org/10.1146/annurev-anchem-061417-125811.

(7) Ranallo, S.; Porchetta, A.; Ricci, F. DNA-Based Scaffolds for Sensing Applications. *Anal. Chem.* **2019**, *91* (1), 44–59. https://doi.org/10.1021/acs.analchem.8b05009.

(8) Pellitero, M. A.; Shaver, A.; Arroyo-Currás, N. Critical Review—Approaches for the Electrochemical Interrogation of DNA-Based Sensors: A Critical Review. *J. Electrochem. Soc.* **2019**, *167* (3), 37529. https://doi.org/10.1149/2.0292003jes.

(9) Arroyo-Currás, N.; Somerson, J.; Vieira, P. A.; Ploense, K. L.; Kippin, T. E.; Plaxco, K. W. Real-Time Measurement of Small Molecules Directly in Awake, Ambulatory Animals. *Proc. Natl. Acad. Sci.* **2017**, *114* (4), 645–650. https://doi.org/10.1073/pnas.1613458114.

(10) Xiao, Y.; Lubin, A. A.; Heeger, A. J.; Plaxco, K. W. Label-Free Electronic Detection of Thrombin in Blood Serum by Using an Aptamer-Based Sensor. *Angew. Chemie Int. Ed.* **2005**, *44* (34), 5456–5459. https://doi.org/https://doi.org/10.1002/anie.200500989.

(11) Yousefi, H.; Mahmud, A.; Chang, D.; Das, J.; Gomis, S.; Chen, J. B.; Wang, H.; Been, T.; Yip, L.; Coomes, E.; Li, Z.; Mubareka, S.; McGeer, A.; Christie, N.; Gray-Owen, S.; Cochrane, A.; Rini, J. M.; Sargent, E. H.; Kelley, S. O. Detection of SARS-CoV-2 Viral Particles Using Direct, Reagent-Free Electrochemical Sensing. *J. Am. Chem. Soc.* **2021**, *143* (4), 1722–1727. https://doi.org/10.1021/jacs.0c10810.

(12) Liu, J.; Zhou, H.; Xu, J. J.; Chen, H. Y. An Effective DNA-Based Electrochemical Switch for Reagentless Detection of Living Cells. *Chem. Commun.* **2011**, *47* (15), 4388–4390. https://doi.org/10.1039/c1cc10430f.

(13) Grall, S.; Li, S.; Jalabert, L.; Kim, S. H.; Chovin, A.; Demaille, C.; Clément, N. Electrochemical Shot Noise of a Redox Monolayer. *Phys. Rev. Lett.* **2023**, *130* (21). https://doi.org/10.1103/PhysRevLett.130.218001.

(14) Fontaine, N.; Dauphin-Ducharme, P. Confounding Effects on the Response of Electrochemical Aptamer-Based Biosensors. *Curr. Opin. Electrochem.* **2023**, *41*, 101361. https://doi.org/https://doi.org/10.1016/j.coelec.2023.101361.

(15) Anne, A.; Bouchardon, A.; Moiroux, J. 3′-Ferrocene-Labeled Oligonucleotide Chains End-Tethered to Gold Electrode Surfaces: Novel Model Systems for Exploring Flexibility of Short DNA Using Cyclic Voltammetry. *J. Am. Chem. Soc.* **2003**, *125* (5), 1112–1113. https://doi.org/10.1021/ja028640k.

(16) Anne, A.; Demaille, C. Dynamics of Electron Transport by Elastic Bending of Short DNA Duplexes. Experimental Study and Quantitative Modeling of the Cyclic Voltammetric Behavior of 3′-Ferrocenyl DNA End-Grafted on Gold. *J. Am. Chem. Soc.* **2006**, *128*, 542–557. https://doi.org/10.1021/ja055112a.

(17) Heeger, A. J.; Lubin, A. A.; Lai, R. Y.; Plaxco, K. W.; Xiao, Y.; Soh, H. T.; Ferguson, B. S.; Swensen, J. S. Continuous, Real-Time Monitoring of Cocaine in Undiluted Blood Serum via a Microfluidic, Electrochemical Aptamer-Based Sensor. *J. Am. Chem. Soc.* **2009**, *131* (12), 4262–4266. https://doi.org/10.1021/ja806531z.

(18) Uzawa, T.; Cheng, R. R.; White, R. J.; Makarov, D. E.; Plaxco, K. W. A Mechanistic Study of Electron Transfer from the Distal Termini of Electrode-Bound, Single-Stranded DNAs. *J. Am. Chem. Soc.* **2010**, *132* (45), 16120–16126. https://doi.org/10.1021/ja106345d.

(19) Abi, A.; Ferapontova, E. E. Unmediated by DNA Electron Transfer in Redox-Labeled DNA Duplexes End-Tethered to Gold Electrodes. *J. Am. Chem. Soc.* **2012**, *134* (35), 14499–14507. https://doi.org/10.1021/ja304864w.

(20) Dauphin-Ducharme, P.; Arroyo-Currás, N.; Adhikari, R.; Somerson, J.; Ortega, G.; Makarov, D. E.; Plaxco, K. W. Chain Dynamics Limit Electron Transfer from Electrode-Bound, Single-Stranded Oligonucleotides. *J. Phys. Chem. C* **2018**, *122* (37), 21441–21448. https://doi.org/10.1021/acs.jpcc.8b06111.

(21) Dauphin-Ducharme, P.; Arroyo-Currás, N.; Plaxco, K. W. High-Precision Electrochemical Measurements of the Guanine-, Mismatch-, and Length-Dependence of Electron Transfer from Electrode-Bound DNA Are Consistent with a Contact-Mediated Mechanism. *J. Am. Chem. Soc.* **2019**, *141* (3), 1304–1311. https://doi.org/10.1021/jacs.8b11341.

(22) Farjami, E.; Campos, R.; Ferapontova, E. E. Effect of the DNA End of Tethering to Electrodes on Electron Transfer in Methylene Blue-Labeled DNA Duplexes. *Langmuir* **2012**, *28* (46), 16218–16226. https://doi.org/10.1021/la3032336.

(23) Huang, K. C.; White, R. J. Random Walk on a Leash: A Simple Single-Molecule Diffusion Model for Surface-Tethered Redox Molecules with Flexible Linkers. *J. Am. Chem. Soc.* **2013**, *135* (34), 12808–12817. https://doi.org/10.1021/ja4060788.

(24) Hüsken, N.; Gębala, M.; La Mantia, F.; Schuhmann, W.; Metzler-Nolte, N. Mechanistic Studies of Fc-PNA(·DNA) Surface Dynamics Based on the Kinetics of Electron-Transfer Processes. *Chem. - A Eur. J.* **2011**, *17* (35), 9678–9690. https://doi.org/10.1002/chem.201003764.

(25) Zheng, Z.; Kim, S. H.; Chovin, A.; Clement, N.; Demaille, C. Electrochemical Response of Surface-Attached Redox DNA Governed by Low Activation Energy Electron Transfer Kinetics. *Chem. Sci.* **2023**, *14* (13), 3652–3660. https://doi.org/10.1039/d3sc00320e.

(26) Anderson, Larry, B.; Reilley, Charles, N. Thin-Layer Electrochemistry: Steady-State Methods of Studying Rate Processes. *J. Electroanal. Chem.* **1965**, *10*, 295–305.

(27) Kang, S.; Nieuwenhuis, A. F.; Mathwig, K.; Mampallil, D.; Lemay, S. G. Electrochemical Single-Molecule Detection in Aqueous Solution Using Self-Aligned Nanogap Transducers. *ACS Nano* **2013**, *7* (12), 10931–10937. https://doi.org/10.1021/nn404440v.

(28) Wolfrum, B.; Kätelhön, E.; Yakushenko, A.; Krause, K. J.; Adly, N.; Hüske, M.; Rinklin, P. Nanoscale Electrochemical Sensor Arrays: Redox Cycling Amplification in Dual-Electrode Systems. *Acc. Chem. Res.* **2016**, *49* (9), 2031–2040. https://doi.org/10.1021/acs.accounts.6b00333.

(29) White, H. S.; McKelvey, K. Redox Cycling in Nanogap Electrochemical Cells. *Curr. Opin. Electrochem.* **2018**, *7*, 48–53. https://doi.org/10.1016/j.coelec.2017.10.021.

(30) Ma, C.; Contento, N. M.; Gibson, L. R. I. I.; Bohn, P. W. Redox Cycling in Nanoscale-Recessed Ring-Disk Electrode Arrays for Enhanced Electrochemical Sensitivity. *ACS Nano* **2013**, *7* (6), 5483–5490. https://doi.org/10.1021/nn401542x.

(31) Fan, F. R. F.; Bard, A. J. Electrochemical Detection of Single Molecules. *Science (80-.).* **1995**, *267* (5199), 871–874. https://doi.org/10.1126/science.267.5199.871.

(32) Sun, P.; Mirkin, M. V. Electrochemistry of Individual Molecules in Zeptoliter Volumes. *J. Am. Chem. Soc.* **2008**, *130* (26), 8241–8250. https://doi.org/10.1021/ja711088j.

(33) Byers, J. C.; Paulose Nadappuram, B.; Perry, D.; McKelvey, K.; Colburn, A. W.; Unwin, P. R. Single Molecule Electrochemical Detection in Aqueous Solutions and Ionic Liquids. *Anal. Chem.* **2015**, *87*, 10450–10456. https://doi.org/10.1021/acs.analchem.5b02569.

(34) Fu, K.; Kwon, S. R.; Han, D.; Bohn, P. W. Single Entity Electrochemistry in Nanopore Electrode Arrays: Ion Transport Meets Electron Transfer in Confined Geometries. *Acc. Chem. Res.* **2020**, *53* (4), 719–728. https://doi.org/10.1021/acs.accounts.9b00543.

(35) Gupta, N. K.; Wilkinson, E. A.; Karuppannan, S. K.; Bailey, L.; Vilan, A.; Zhang, Z.; Qi, D. C.; Tadich, A.; Tuite, E. M.; Pike, A. R.; Tucker, J. H. R.; Nijhuis, C. A. Role of Order in the Mechanism of Charge Transport across Single-Stranded and Double-Stranded DNA Monolayers in Tunnel Junctions. *J. Am.*

Chem. Soc. **2021**, *143* (48), 20309–20319. https://doi.org/10.1021/jacs.1c09549.

(36) Steentjes, T.; Sarkar, S.; Jonkheijm, P.; Lemay, S. G.; Huskens, J. Electron Transfer Mediated by Surface-Tethered Redox Groups in Nanofluidic Devices. *Small* **2017**, *13* (8), 1603268. https://doi.org/https://doi.org/10.1002/smll.201603268.

(37) Wang, K.; Goyer, C.; Anne, A.; Demaille, C. Exploring the Motional Dynamics of End-Grafted DNA Oligonucleotides by in Situ Electrochemical Atomic Force Microscopy. *J. Phys. Chem. B* **2007**, *111* (21), 6051–6058. https://doi.org/10.1021/jp070432x.

(38) Anne, A.; Bonnaudat, C.; Demaille, C.; Wang, K. Enzymatic Redox 3′-End-Labeling of DNA Oligonucleotide Monolayers on Gold Surfaces Using Terminal Deoxynucleotidyl Transferase (TdT)-Mediated Single Base Extension. *J. Am. Chem. Soc.* **2007**, *129*, 2734–2735. https://doi.org/10.1021/ja067954v.

(39) Madrid, I.; Zheng, Z.; Gerbelot, C.; Fujiwara, A.; Li, S.; Grall, S.; Nishiguchi, K.; Kim, S.-H.; Chovin, A.; Demaille, C.; Clement, N. Ballistic Brownian Motion of Nanoconfined DNA. *ACS Nano* **2023**, *17* (17), 17031–17040. https://doi.org/10.1021/acsnano.3c04349.

(40) Levicky, R.; Herne, T. M.; Tarlov, M. J.; Satija, S. K. Using Self-Assembly To Control the Structure of DNA Monolayers on Gold: A Neutron Reflectivity Study. *J. Am. Chem. Soc.* **1998**, *120* (38), 9787–9792. https://doi.org/10.1021/ja981897r.

(41) Ge, D.; Levicky, R. A Comparison of Five Bioconjugatable Ferrocenes for Labeling of Biomolecules. *Chem. Commun.* **2010**, *46* (38), 7190–7192. https://doi.org/10.1039/C0CC02044C.

(42) Mills, J. B.; Vacano, E.; Hagerman, P. J. Flexibility of Single-Stranded DNA: Use of Gapped Duplex Helices to Determine the Persistence Lengths of Poly(DT) and Poly(DA). *J. Mol. Biol.* **1999**, *285* (1), 245–257. https://doi.org/10.1006/jmbi.1998.2287.

(43) Doose, S.; Barsch, H.; Sauer, M. Polymer Properties of Polythymine as Revealed by Translational Diffusion. *Biophys. J.* **2007**, *93* (4), 1224–1234. https://doi.org/10.1529/biophysj.107.107342.

(44) Chen, H.; Meisburger, S. P.; Pabit, S. A.; Sutton, J. L.; Webb, W. W.; Pollack, L. Ionic Strength-Dependent Persistence Lengths of Single-Stranded RNA and DNA. *Proc. Natl. Acad. Sci.* **2012**, *109* (3), 799–804. https://doi.org/10.1073/pnas.1119057109.

(45) Anne, A.; Bonnaudat, C.; Demaille, C.; Wang, K. Enzymatic Redox 3′-End-Labeling of DNA Oligonucleotide Monolayers on Gold Surfaces Using Terminal Deoxynucleotidyl Transferase (TdT)-Mediated Single Base Extension. *J. Am. Chem. Soc.* **2007**, *129* (10), 2734–2735. https://doi.org/10.1021/ja067954v.

(46) Chi, Q.; Wang, G.; Jiang, J. The Persistence Length and Length per Base of Single-Stranded DNA Obtained from Fluorescence Correlation Spectroscopy Measurements Using Mean Field Theory. *Phys. A Stat. Mech. its Appl.* **2013**, *392* (5), 1072–1079. https://doi.org/https://doi.org/10.1016/j.physa.2012.09.022.

(47) Snodin, B. E. K.; Randisi, F.; Mosayebi, M.; Šulc, P.; Schreck, J. S.; Romano, F.; Ouldridge, T. E.; Tsukanov, R.; Nir, E.; Louis, A. A.; Doye, J. P. K. Introducing Improved Structural Properties and Salt Dependence into a Coarse-Grained Model of DNA. *J. Chem. Phys.* **2015**, *142* (23), 234901. https://doi.org/10.1063/1.4921957.

(48) Stellwagen, N. C.; Magnusdottir, S.; Gelfi, C.; Righetti, P. G. Measuring the Translational Diffusion Coefficients of Small DNA Molecules by Capillary Electrophoresis. *Biopolymers* **2001**, *58* (4), 390–397. https://doi.org/https://doi.org/10.1002/1097-0282(20010405)58:4<390::AID-BIP1015>3.0.CO;2-K.

(49) Ortega, A.; Garcia De La Torre, J. Hydrodynamic Properties of Rodlike and Dislike Particles in Dilute Solution. *J. Chem. Phys.* **2003**, *119* (18), 9914–9919. https://doi.org/10.1063/1.1615967.

(50) Langer, A.; Kaiser, W.; Svejda, M.; Schwertler, P.; Rant, U. Molecular Dynamics of DNA-Protein Conjugates on Electrified Surfaces: Solutions to the Drift-Diffusion Equation. *J. Phys. Chem. B* **2014**, *118* (2), 597–607. https://doi.org/10.1021/jp410640z.

(51) Wang, K.; Goyer, C.; Anne, A.; Demaille, C. Exploring the Motional Dynamics of End-Grafted DNA Oligonucleotides by in Situ Electrochemical Atomic Force Microscopy. *J. Phys. Chem. B* **2007**, *111*, 6051–6058. https://doi.org/10.1021/jp070432x.

(52) White, R. J.; White, H. S. Electrochemistry in Nanometer-Wide Electrochemical Cells. *Langmuir* **2008**, *24* (6), 2850–2855. https://doi.org/10.1021/la7031779.

(53) Kim, J.; Shen, M.; Nioradze, N.; Amemiya, S. Stabilizing Nanometer Scale Tip-to-Substrate Gaps in Scanning Electrochemical Microscopy Using an Isothermal Chamber for Thermal Drift Suppression. *Anal. Chem.* **2012**, *84* (8), 3489–3492. https://doi.org/10.1021/ac300564g.

(54) Fleming, S. J.; Lu, B.; Golovchenko, J. A. Charge, Diffusion, and Current Fluctuations of Single-Stranded DNA Trapped in an MspA Nanopore. *Biophys. J.* **2017**, *112* (2), 368–375. https://doi.org/https://doi.org/10.1016/j.bpj.2016.12.007.

(55) Chen, Q.; McKelvey, K.; Edwards, M. A.; White, H. S. Redox Cycling in Nanogap Electrochemical Cells. The Role of Electrostatics in Determining the Cell Response. *J. Phys. Chem. C* **2016**, *120* (31), 17251–17260. https://doi.org/10.1021/acs.jpcc.6b05483.

(56) Bae, J. H.; Yu, Y.; Mirkin, M. V. Diffuse Layer Effect on Electron-Transfer Kinetics Measured by Scanning Electrochemical Microscopy (SECM). *J. Phys. Chem. Lett.* **2017**, *8* (7), 1338–1342. https://doi.org/10.1021/acs.jpclett.7b00161.

(57) Tan, S.; Perry, D.; Unwin, P. R. Double Layer Effects in Voltammetric Measurements with Scanning Electrochemical Microscopy (SECM). *J. Electroanal. Chem.* **2018**, *819*, 240–250. https://doi.org/https://doi.org/10.1016/j.jelechem.2017.10.044.

(58) Abbou, J.; Anne, A.; Demaille, C. Probing the Structure and Dynamics of End-Grafted Flexible Polymer Chain Layers by Combined Atomic Force-Electrochemical Microscopy. Cyclic Voltammetry within Nanometer-Thick Macromolecular Poly(Ethylene Glycol) Layers. *J. Am. Chem. Soc.* **2004**, *126* (32), 10095–10108. https://doi.org/10.1021/ja0493502.

(59) Zevenbergen, M. A. G.; Wolfrum, B. L.; Goluch, E. D.; Singh, P. S.; Lemay, S. G. Fast Electron-Transfer Kinetics Probed in Nanofluidic Channels. *J. Am. Chem. Soc.* **2009**, *131* (32), 11471–11477. https://doi.org/10.1021/ja902331u.

(60) Chidsey, C. E. D. Free Energy and Temperature Dependence of Electron Transfer at the Metal-Electrolyte Interface. *Science (80-.).* **1991**, *4996* (251), 919–922. https://doi.org/10.1126/science.251.4996.919.

(61) Marcus, R. A. On the Theory of Electron-Transfer Reactions. VI. Unified Treatment for Homogeneous and Electrode Reactions. *J. Chem. Phys.* **1965**, *43* (2), 679–701. https://doi.org/10.1063/1.1696792.

(62) Savéant, J.-M. Effect of the Electrode Continuum of States in Adiabatic and Nonadiabatic Outer-Sphere and Dissociative Electron Transfers. Use of Cyclic Voltammetry for Investigating Nonlinear Activation-Driving Force Laws. *J. Phys. Chem. B* **2002**, *106* (36), 9387–9395. https://doi.org/10.1021/jp0258006.

(63) Paul, A.; Borrelli, R.; Bouyanfif, H.; Gottis, S.; Sauvage, F. Tunable Redox Potential, Optical Properties, and Enhanced Stability of Modified Ferrocene-Based Complexes. *ACS Omega* **2019**, *4* (12), 14780–14789. https://doi.org/10.1021/acsomega.9b01341.

(64) Bonthuis, D. J.; Gekle, S.; Netz, R. R. Dielectric Profile of Interfacial Water and Its Effect on Double-Layer Capacitance. *Phys. Rev. Lett.* **2011**, *107* (16), 166102. https://doi.org/10.1103/PhysRevLett.107.166102.

(65) Bangle, R. E.; Schneider, J.; Conroy, D. T.; Aramburu-Trošelj, B. M.; Meyer, G. J. Kinetic Evidence That the Solvent Barrier for Electron Transfer Is Absent in the Electric Double Layer. *J. Am. Chem. Soc.* **2020**, *142* (35), 14940–14946. https://doi.org/10.1021/jacs.0c05226.

(66) Fumagalli, L.; Esfandiar, A.; Fabregas, R.; Hu, S.; Ares, P.;

Janardanan, A.; Yang, Q.; Radha, B.; Taniguchi, T.; Watanabe, K.; Gomila, G.; Novoselov, K. S.; Geim, A. K. Anomalously Low Dielectric Constant of Confined Water. *Science (80-.).* **2018**, *360* (6395), 1339–1342. https://doi.org/10.1126/science.aat4191.

(67) Smalley, J. F.; Finklea, H. O.; Chidsey, C. E. D.; Linford, M. R.; Creager, S. E.; Ferraris, J. P.; Chalfant, K.; Zawodzinsk, T.; Feldberg, S. W.; Newton, M. D. Heterogeneous Electron-Transfer Kinetics for Ruthenium and Ferrocene Redox Moieties through Alkanethiol Monolayers on Gold. *J. Am. Chem. Soc.* **2003**, *125* (7), 2004–2013. https://doi.org/10.1021/ja028458j.

(68) Trasobares, J.; Rech, J.; Jonckheere, T.; Martin, T.; Aleveque, O.; Levillain, E.; Diez-Cabanes, V.; Olivier, Y.; Cornil, J.; Nys, J. P.; Sivakumarasamy, R.; Smaali, K.; Leclere, P.; Fujiwara, A.; Théron, D.; Vuillaume, D.; Clément, N. Estimation of π–π Electronic Couplings from Current Measurements. *Nano Lett.* **2017**, *17*, 3215–3224. https://doi.org/10.1021/acs.nanolett.7b00804.

(69) Hegner, M.; Wagner, P.; Semenza, G. Ultralarge Atomically Flat Template-Stripped Au Surfaces for Scanning Probe Microscopy. *Surf. Sci.* **1993**, *291* (1–2), 39–46. https://doi.org/10.1016/0039-6028(93)91474-4.

(70) Anne, A.; Cambril, E.; Chovin, A.; Demaille, C. Touching Surface-Attached Molecules with a Microelectrode: Mapping the Distribution of Redox-Labeled Macromolecules by Electrochemical-Atomic Force Microscopy. *Anal. Chem.* **2010**, *82*, 6353–6362. https://doi.org/10.1021/ac1012464.

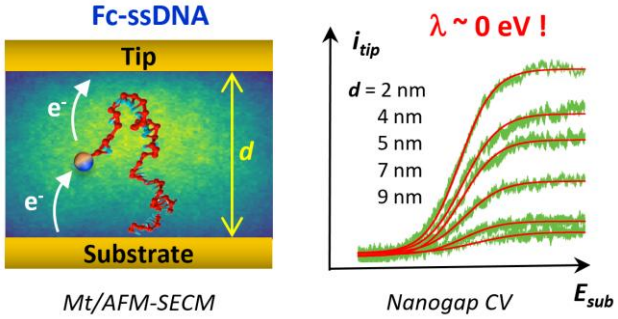
Fc-ssDNA
Tip
e-
e-
d
Substrate
Mt/AFM-SECM
λ ~ 0 eV !
itip
d = 2 nm
4 nm
5 nm
7 nm
9 nm
Esub
Nanogap CV